Rare Metal Materials and Engineering
Volume 53, Issue 12, December 2024
Available online at www.rmme.ac.cn

Science Press

Cite this article as: Liu Na, Zhao Zhanglong, Liu Yuli, et al. Formation of Sub-grain Structure Induced by Composition Segregation and Stacking Faults in Laser-Deposited Premixed Near-α Titanium Alloy and Ti_2AlNb Alloy Powders[J]. Rare Metal Materials and Engineering, 2024, 53(12): 3281-3290. DOI: 10.12442/j.issn.1002-185X.20240097.

ARTICLE

Formation of Sub-grain Structure Induced by Composition Segregation and Stacking Faults in Laser-Deposited Premixed Near-α Titanium Alloy and Ti_2AlNb Alloy Powders

Liu Na[1,2], Zhao Zhanglong[1], Liu Yuli[1,2], Feng Kaikai[3], Zha Xiaohui[3], Li Pu[3], Xu Wenxin[1], Yang Haiou[1,2], Lai Yunjin[4]

[1] School of Materials Science and Engineering, Northwestern Polytechnical University, Xi'an 710072, China; [2] State Key Laboratory of Solidification Processing, Northwestern Polytechnical University, Xi'an 710072, China; [3] Engine Development Department, AECC Hunan Aviation Powerplant Research Institute, Zhuzhou 412002, China; [4] Xi'an Sino-Euro Materials Technologies Co., Ltd, Xi'an 710018, China

Abstract: Near-α titanium alloy and Ti_2AlNb alloy powders premixed with different proportions were prepared on the near-α titanium alloy substrate by laser deposition technique, and the microstructure characteristics were analyzed and discussed. Results show that numerous river-like sub-grain structures are formed inside the equiaxed B2 grains of the laser-deposited premixed titanium alloy powders with the proportion of Ti_2AlNb above 40wt%, whereas the needle-like structure within coarse columnar β grains exist with the proportion of Ti_2AlNb below 40wt%. It is noteworthy that the decrease in laser power and scanning speed can accelerate the formation of sub-grain structures. Based on the analysis of experimental results, it can be inferred that the formation of sub-grain structure not only is related to the precipitation of O phase due to composition micro-segregation at sub-grain boundaries, but also is inseparable from the stacking faults caused by the internal stress during the laser deposition.

Key words: laser deposition; premixed titanium alloy powders; sub-grain structure; composition segregation; stacking faults

With the rapid development of aerospace, nuclear energy, electronics and other industries, the requirements for the high performance components are increasing. Titanium alloys have been widely used in important and advanced aerospace components due to the high specific strength and excellent mechanical properties[1–4]. Compared with single homogeneous titanium alloy components that can only be used at the specific temperature and within stress range, gradient titanium alloy components with smooth variations in composition, microstructure and performance in specific direction have greater engineering application value in the aerospace field[5–6]. Gradient titanium alloy components have the potential advantage of working normally and repeatedly under some harsh conditions. Their excellent properties cannot generally be achieved by conventional manufacturing techniques such as casting or forging[7]. The layer-by-layer laser deposition is an advanced additive manufacturing (AM) technique combined with rapid prototyping and laser cladding, which is attractive to produce titanium alloy components with intricate geometries[8–10]. It has been reported that mechanical properties such as tensile strength can be improved by combining forging and deposition process during titanium alloy manufacturing[11–12]. Therefore, the combination of AM and forging, in which the metallic powders are directly placed on the forged plate, is an effective method for the preparation of gradient titanium alloys. The near-α titanium alloy can effectively ensure the serving temperature of components up to 600 °C for long time. Ti_2AlNb alloy performs prominent high-temperature performance with the working temperature of 650–900 °C. However, it also has the disadvantages of high density and high cost. If the near-α high-temperature titanium alloy and the Ti_2AlNb alloy powders are mixed and then

Received date: February 27, 2024
Foundation item: National Natural Science Foundation of China (51974259); Xi'an Municipal Bureau of Science and Technology (21ZCZZHXJS-QCY6-0008); Industry-Academic Cooperation Project of Aero Engine Corporation of China (HFZL2020CXY021)
Corresponding author: Zhao Zhanglong, Ph. D., Associate Professor, School of Materials Science and Engineering, Northwestern Polytechnical University, Xi'an 710072, P. R. China, E-mail: zlzhao@nwpu.edu.cn

deposited on the forged near-α titanium alloy substrate to prepare gradient titanium alloy, which not only alleviates the sudden change in microstructure and properties of the bonding interface due to direct connection between the two alloys, but also meets the demands of the lightweight surface accompanied by high mechanical properties and low cost. Whereas the complex physical metallurgical process and non-equilibrium solidification with high cooling rate and thermal gradient in laser deposition processes may lead to the preferred crystallographic orientation and the formation of coarse columnar β grains epitaxially grown along the deposition direction in the gradient titanium alloy[13–15]. Columnar grains in laser-deposited gradient titanium alloy components can result in anisotropic mechanical properties which require efforts to avoid.

Attempts to optimize the processing parameters of laser deposition have shown that it is difficult to alter the conditions to promote equiaxed growth of β grains in titanium alloy[16]. Hicks et al[17] indicated that the microstructure of Ti-5553 alloy prepared by laser deposition was predominantly large columnar β-grains aligned with the deposition direction, interspersed with fine equiaxed β-grains. Besides, the increase in the laser power and powder feed rate can reduce the average β-grain size and promote the formation of clusters of fine grains to be retained during the deposition of subsequent layers, but cannot eliminate columnar grains. Though some alloying elements (such as B[18–21], Ni[22], Cu[23–24] and C[25]) and ceramic particles (such as BN[26], ZrB_2[27], Y_2O_3[28], La_2O_3[29] and BNNTs[30]) have been added into titanium alloys to refine β grains, the loss of comprehensive mechanical properties due to the formation of hard particle phases and the inhomogeneous distribution of refined β grains cannot be ignored. Recently, it has been reported that the fully equiaxed grain structure and better mechanical properties were realized in the laser-deposited near-α titanium alloy and Ti_2AlNb alloy powders with different proportions[31]. In addition, the unique sub-grain structures were formed inside β/B2 grains with high Ti_2AlNb content, and similar phenomena usually appeared in the laser-deposited superalloys or steels[32–33].

The existence of sub-grain structures is supposed to have significant impact on the mechanical properties in laser-deposited metal components. Zhao et al[34] demonstrated that the strength and ductility of prepared IN718 alloy with cellular sub-grain structure were simultaneously improved compared with those of the alloy without cellular sub-grain structure, which even exceeded the mechanical properties standards of wrought IN718 alloy. Salman et al[35] illustrated that the complex cellular structure and sub-grains could contribute to the higher strength and better ductility of the selective laser melted samples in comparison with the results of annealed samples. Therefore, it is necessary to investigate the formation mechanism of sub-grain structure in laser-deposited gradient titanium alloy. Recent reports showed the formation mechanism of sub-grain structure in laser additive manufactured superalloys and steels. For example, Saeidi et al[32] indicated that the formation of columnar sub-grain structure inside each individual large grain was attributed to the compositional fluctuation induced by large Mo atoms of quenched austenite steel during the laser melting. Cao et al[33] pointed that deformation of cellular grains caused by crystallographic defects and compositional segregation was the main reason for the formation of sub-grain structures in laser additive manufacturing of IN718 alloy. Liu et al[36] founded that river-like sub-grain boundaries were formed inside the laser melting-deposited B2 grains of Ti_2AlNb-based alloy, but the formation mechanism of the sub-grain was unclear.

In this study, to explore the feasibility of preparing gradient titanium alloys by AM-forging technique, powders of near-α titanium alloy and Ti_2AlNb alloy premixed with different proportions were deposited on the forged near-α titanium alloy substrate by laser deposition. The investigation specifically focused on elucidating the microstructural evolution of β/B2 grains with the introduction of Ti_2AlNb alloy, which leads to the formation of sub-grain structures within individual grains. The microstructure evolution, composition distribution and phase structure were observed by optical microscope (OM), scanning electron microscope (SEM) and transmission electron microscope (TEM). These meticulous research findings are critical for understanding the formation process of sub-grain structure due to compositional segregation and the presence of stacking faults. Besides, the foundation will be made for controlling sub-grain structures to optimize the properties of gradient titanium alloys during the laser deposition process.

1 Experiment

The raw materials were spherical near-α titanium alloy (Ti-5.8Al-4.8Sn-2Zr-1Mo-0.35Si-0.85Nd) powders with the diameter of 74–178 μm and spherical Ti_2AlNb alloy powders with the diameter of 53–150 μm. The morphologies and particle size distribution of the two powders are shown in Fig. 1. The chemical composition of the two powders is presented in Table 1. The near-α titanium alloy and Ti_2AlNb alloy powders were prepared by super-speed plasma rotating electrode technique. Near-α titanium alloy and Ti_2AlNb alloy powders with different proportions were fully premixed in the planetary ball mill for 2 h (forward rotation for 5 min, reverse rotation for 5 min, and then repetition of the cycle) to ensure the uniformity of powders. Subsequently, the premixed titanium alloy powders (Ti_2AlNb alloy proportions were 10wt% – 90wt% with 5wt% increment) were dried in the vacuum drying oven at 120±10 ºC for 4 h for the laser deposition process. The forged near-α titanium alloy plate was chosen as the substrate, and it was polished to remove the oxide layers before laser deposition.

The laser deposition experiments were conducted by the developed LSF-VI system equipped with the semiconductor laser (maximum output power 6000 W), the DPSF-2 power feeder together with co-axial powder delivery nozzle, computer numerical control multi-axis motion system, and vacuum chamber. The laser deposition process was conducted under constant flow of ultra-high purity Ar to minimize the

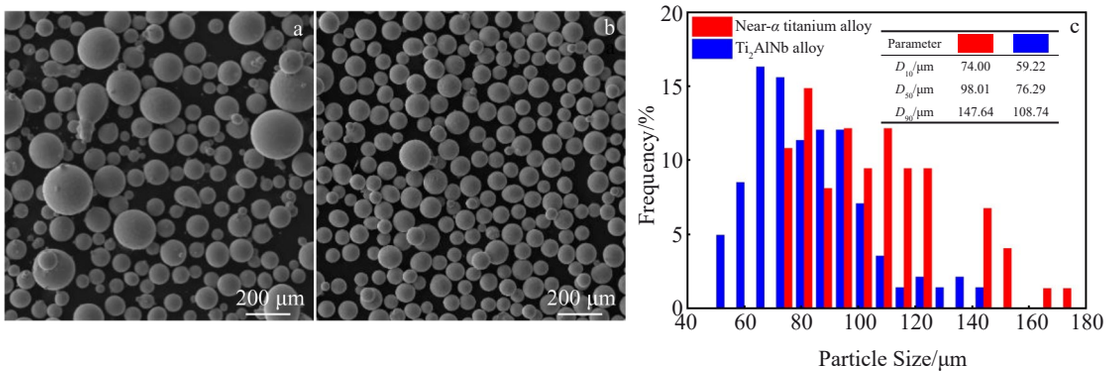

Fig.1 Morphologies (a–b) and particle size distribution (c) of different powders: (a) near-α titanium alloy and (b) Ti_2AlNb alloy

Table 1 Chemical composition of Ti_2AlNb and near-α titanium alloy powders (wt%)

Powder	Al	Sn	Zr	Mo	Si	Ta	Nb	Ti
Ti_2AlNb alloy	22.24	-	-	-	-	-	25.12	Bal.
Near-α titanium alloy	6.14	3.68	3.43	0.52	0.55	0.96	0.40	Bal.

oxygen contamination (residual oxygen concentration under 50×10^{-3}vol%). The forged near-α titanium alloy substrate was fixed on the horizontal workbench (along *X*-*Y* direction), and the premixed titanium alloy powders were fed into the molten pool produced by laser beam. The molten metal powder was solidified on the substrate, and then deposition layers were formed with the stepped movement of laser beam and powder feed head in the *Z*-direction. The detailed working principle of the laser deposition system is shown in Fig. 2a. To reduce the thermal stress during the laser deposition process, the reciprocating laser scanning strategy that scanning was bi-directional and the scanning direction was kept 90° between the two successive layers was adopted. Based on research and previous experiments, the processing parameters of laser deposition were selected as follows: the laser power of 2600–3000 W, the scanning speed of 800 and 1000 mm/min, the powder feeding of 7.37 g/min, the beam diameter of 3 mm, the overlap rate of 50%, the increment along the *Z*-axis of 0.3 mm. The appearances of as-deposited bulk samples with the size of 20 mm×5 mm×5 mm are shown in Fig.2b.

After laser deposition, the samples were cut along the laser scanning direction and parallelled to the deposition direction. Metallographic microstructure was characterized by OM (OLYMPUS GX-71) after being etched with the Kroll's etching solution of 10 mL HF+15 mL H_2O_2+35 mL HNO_3+ 100 mL H_2O at room temperature for 30 s. The grain sizes and distribution of sub-grains structure were analyzed by SEM (MIRA3 TESCAN) with the electron backscattered diffractometer (EBSD). The recorded data were analyzed by the KHL Channel 5 software. The composition distribution around the sub-grain boundary was measured by SEM (G3 UC) equipped with energy dispersive spectroscope (EDS). Detailed microstructure and phase structure analysis were executed by TEM (Talos F200X) equipped with EDS, which could measure the compositional micro-segregation of precipitate phases.

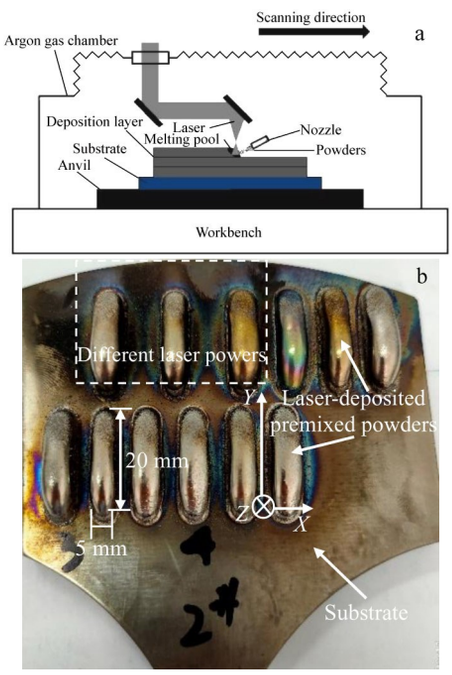

Fig.2 Schematic diagram of laser deposition (a) and different laser-deposited bulk samples (b)

2 Results and Discussion

2.1 Formation of sub-grain structure inside equiaxed grains with increase in Ti_2AlNb content

Fig. 3 shows the microstructures of as-deposited near-α titanium alloy and Ti_2AlNb alloy premixed powders with different proportions. Large columnar prior-β grains with the length>2.5 mm and the width>300 μm can be observed in the laser-deposited premixed powders with 10wt%

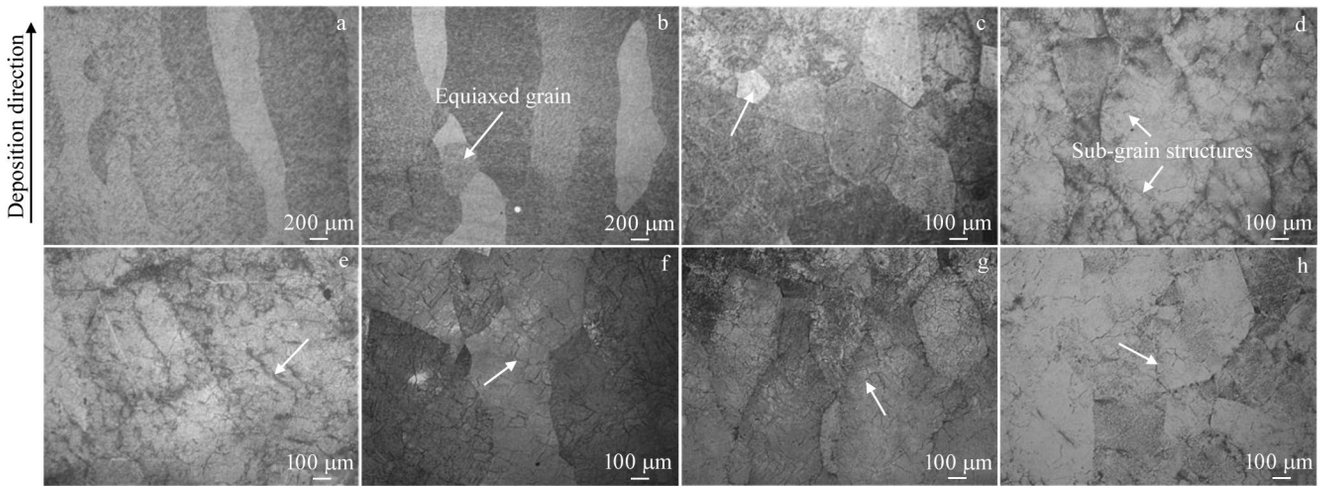

Fig.3 Microstructures of the laser-deposited premixed powders with different proportions of Ti_2AlNb alloy: (a) 10wt%; (b) 30wt%; (c) 35wt%; (d) 40wt%; (e) 45wt%; (f) 50wt%; (g) 70wt%; (h) 90wt%

Ti_2AlNb, as shown in Fig.3a. When the proportion of Ti_2AlNb is increased to 30wt%, the small equiaxed β grains (white arrows) with the diameter<200 μm are observed, and the large columnar β grains with the width>500 μm and the length>2.5 mm still can be identified in Fig. 3b. When the proportion of Ti_2AlNb exceeds 30wt%, significant changes occur. As shown in Fig.3c–3h, large columnar β grains clearly disappear and plentiful equiaxed grains with the maximum grain diameter<500 μm are formed. This transition indicates that with the increase in Ti_2AlNb alloy content, the grain morphology changes from predominantly columnar to more equiaxed structure, accompanied with the general decrease in grain size towards finer and more uniform distribution.

Moreover, it is noteworthy that unique river-like sub-grain structures (arrows in Fig.3d–3h) are observed within the equiaxed B2 grains of the laser-deposited premixed powders when the Ti_2AlNb proportion is above 40wt%. The distinctive microstructural features are probably helpful in enhancing mechanical strength and improving ductility and fatigue resistance in laser-deposited titanium alloy[32].

EBSD analysis was performed to study the microstructure inside B2 grains of the laser-deposited premixed titanium alloy powders with different proportions of Ti_2AlNb, and the results are shown in Fig. 4. As shown in Fig. 4a – 4b, the microstructure of the laser-deposited premixed titanium alloy powders with 10wt% Ti_2AlNb is composed of large columnar β grains and some small-sized equiaxed β grains with needle-like martensite and α_2 phases uniformly precipitated from the α matrix phases inside the grains. Massive flake clusters with similar orientations are observed from the inverse pole figures (IPFs) in Fig. 4c – 4d, which indicates that the strong variant-selective preference for the $\beta \rightarrow \alpha$ phase transformation occurs during cooling process of the laser deposition. When the Ti_2AlNb proportion increase to 70wt% (Fig. 4e – 4f), the band contrast (BC) figure and IPF exhibit that the large equiaxed B2 grains are composed of fine sub-grains, which take similar crystallographic orientation within each large polycrystalline grain. As depicted in Fig. 4g, the laser-deposited premixed powders with 70wt% Ti_2AlNb shows refined structure composed of small sub-grains. The values recorded on the kernel average misorientation angle (KAM) map can accurately reflect the differences in lattice orientation between each sub-grain in refined structure and the resulting distribution of plastic strain. This unique microstructure with the low angle grain boundaries (LAGBs), accounting for 31.92%, reflects that the addition of Ti_2AlNb can effectively refine the grains in controlled manner, as shown in Fig. 4h. The proportion of high angle grain boundaries (HAGBs) is also shown in Fig. 4h. In conclusion, the increase in Ti_2AlNb proportion not only leads to significant decrease in the size of columnar β grains but also refines the grains characterized by well-oriented sub-grains.

2.2 Sub-grain structure under different laser deposition parameters

To further study the sub-grain structure, the microstructures of premixed powders with 50wt% Ti_2AlNb alloy prepared under different laser deposition processing parameters are displayed in Fig. 5. When the laser power is 2600 W and scanning speed is 1000 mm/min (Fig.5a), the microstructure is mainly composed of equiaxed B2 grains with the grain size of about 373 μm. The sizes and distributions of sub-grains vary obviously in different areas of individual B2 grains, in which the small-sized sub-grains are concentrated on the trigeminal grain boundaries. When the laser power is increased from 2800 W to 3000 W, the B2 grain size increases from around 409 μm to 429 μm. But the volume fraction of sub-grains is significantly decreased, as indicated in Fig.5b–5c. In addition, when the laser power is 3000 W and the scanning speed is decreased from 1000 mm/min to 800 mm/min, the B2 grain size increases from about 429 μm to 449 μm. The volume fraction of sub-grains also increases, as shown in Fig. 5c – 5d. Obviously, the B2 grain sizes and the volume

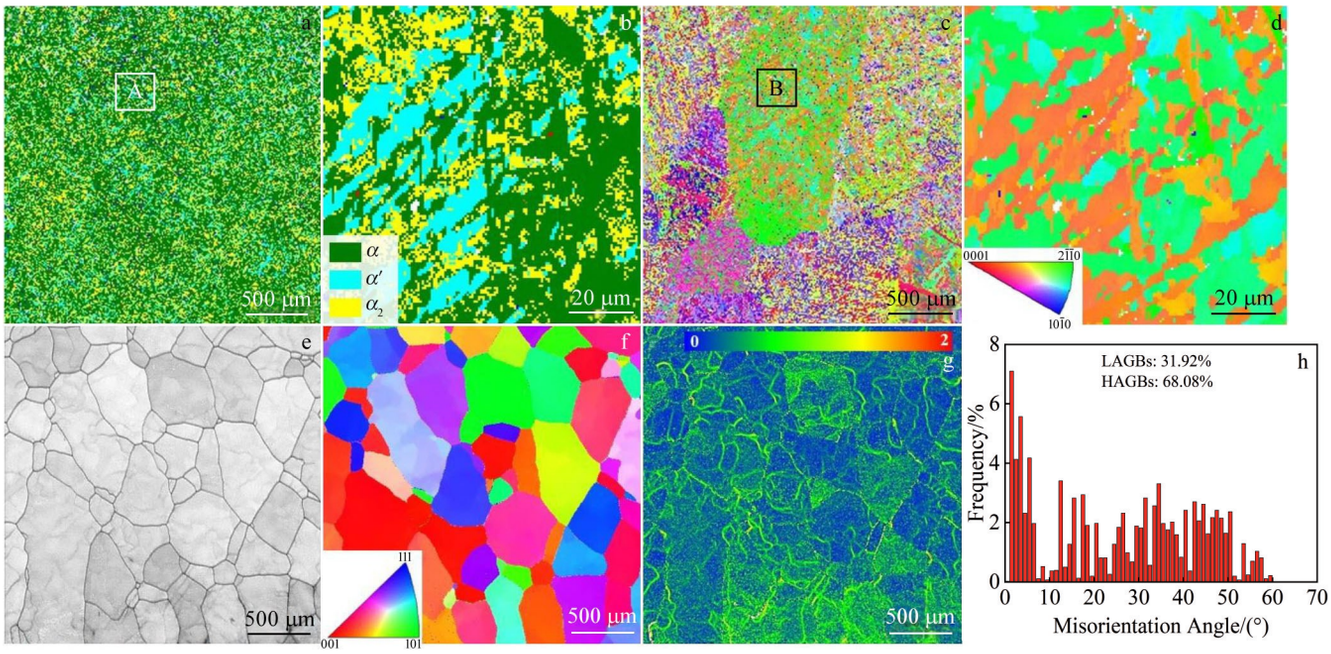

Fig.4 EBSD microstructures of laser-deposited premixed powders with 30wt% (a–d) and 70wt% (e–h) Ti_2AlNb alloy: (a) phase; (b) magnified image of region A in Fig.4a; (c, f) IPF; (d) magnified image of region B in Fig.4c; (e) BC figure; (g) KAM map; (h) grain boundaries distribution

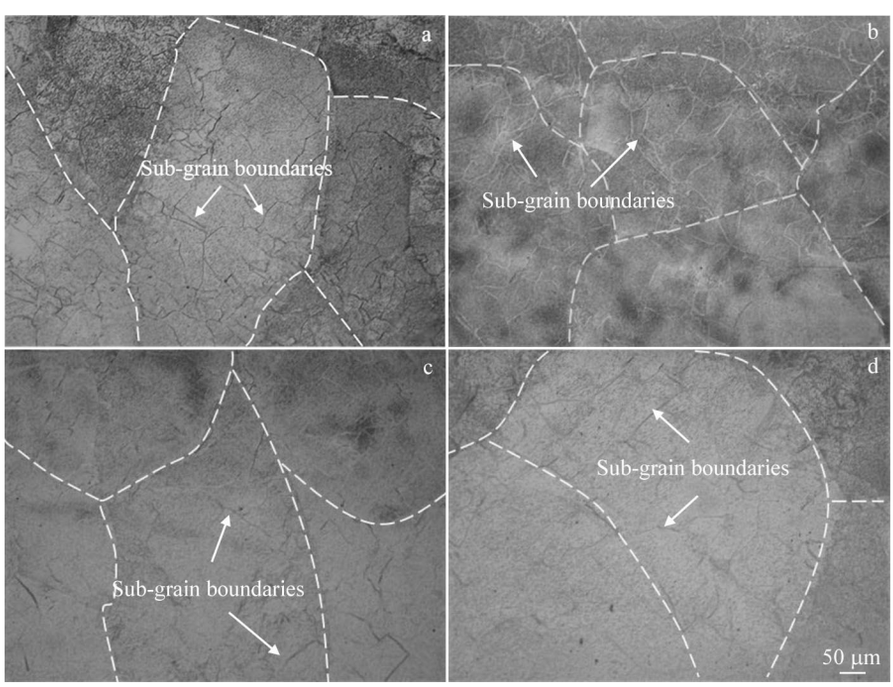

Fig.5 Microstructures of laser-deposited premixed powders with 50wt% Ti_2AlNb alloy prepared under different laser deposition processing parameters: (a) 2600 W, 1000 mm/min; (b) 2800 W, 1000 mm/min; (c) 3000 W, 1000 mm/min; (d) 3000 W, 800 mm/min

fraction of sub-grains are sensitive to laser deposition processing parameters. The increase in laser power and the decrease in scanning speed can accelerate the growth of B2 grains, whereas the increase in both laser power and scanning speed can inhibit the formation of sub-grain structures.

The orientation characteristics of the sub-grains in the laser-deposited premixed titanium alloy powders with the Ti_2AlNb proportion of 50wt% are shown in Fig.6. It is not difficult to find from BC figure and IPF that the river-like sub-grains with similar orientation are formed inside the B2 grains. According to the quantitative analysis of grain boundaries (Fig.6d), the frequency of LAGBs i.e., the local misorientation is less than 15°, is 34.86%. It can be easily inferred that the LAGBs are

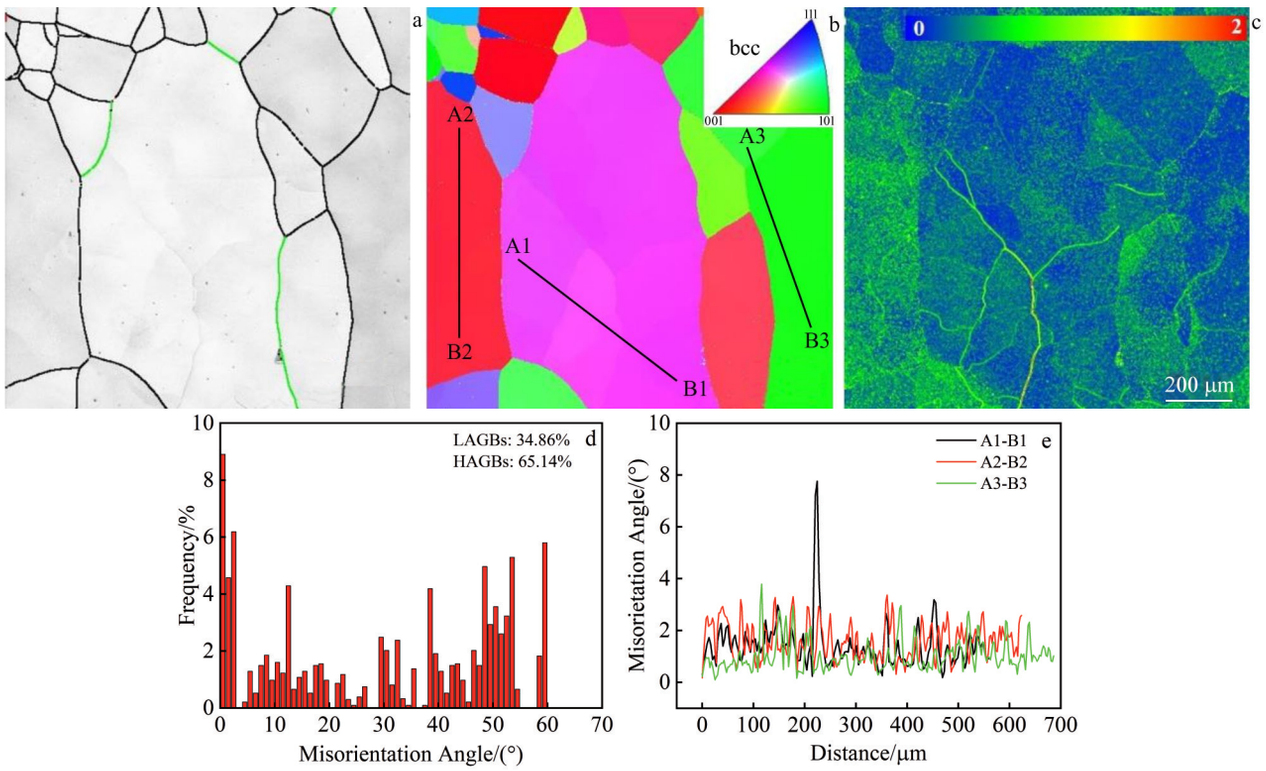

Fig.6 EBSD results of laser-deposited premixed titanium alloy powders with Ti_2AlNb proportion of 50wt%: (a) BC figure; (b) IPF; (c) KAM map; (d) grain boundaries distribution; (e) misorientation variation with lines in Fig.6b

the main sub-structure of coarse B2 grains. Fig.6e shows the distribution of the local misorientation angle in three random directions of the B2 grains. The maximum value of the local misorientation angle in different columnar grains is different and can reach 7.07° (line A1-B1). It can be determined that the peak point of the local misorientation is the point of the sub-structure boundary. It is well known that the KAM maps can be used to estimate the plastic strain. The higher value of KAMs mainly focus on the sub-grain structures inside the B2 grains with lots of LAGBs in them, indicating the existence of internal stress.

2.3 Composition segregation at sub-grain boundary

It is noted that the sub-grain structures are formed inside equiaxed grains of the laser-deposited premixed titanium alloy powders with the proportions of Ti_2AlNb above 40wt%. The formation of equiaxed grains is closely related to constitutional supercooling caused by the changes in solute concentration ahead of the solid-liquid interface. For most of laser-deposited titanium alloys, constitutional supercooling is not expected to be significant enough to cause the nucleation of equiaxed dendrites.

However, with the presence of potent heterogeneous nucleation, the alloying elements are important for the formation of equiaxed dendrites. The relative contribution of alloying elements to constitutional supercooling can be quantified by the growth restriction factor Q[13], as follows:

$$Q = m_1 c_0 (k-1) \quad (1)$$

where m_1 is the slope of liquid line, c_0 is the solute concentration, and k is the solute partition coefficient.

The values of $m_1(k-1)$ for different solute elements in titanium alloys are calculated by Ti-X binary-phase diagrams, as listed in Table 2[37–38]. It can be seen that the partition coefficients of Al, V, Sn and Zr are about 1, which makes constitutional supercooling resulting from the Q values insufficiently enough to lead to the nucleation of equiaxed grains ahead of the solid-liquid interface. Thus, the formation of equiaxed grains is very rare in laser-deposited titanium alloys. In addition, the contents of Si and Mo elements for the near-α titanium alloy are about 0.35% and 1%, respectively. So the Q values of Si and Mo are less than 6.5 K for mixed powders with Ti_2AlNb alloy. However, Nb element is the promising solute in titanium alloy with the maximum of c_0 as high as 15wt% and the value of $m_1(k-1)$ as high as 6.6 K. It leads to very high maximum Q value of Nb element, which further surpasses that of Si or Mo elements. Therefore, equiaxed grains are much easier to obtain in the laser-deposited premixed titanium alloy powders with higher Nb content than with lower Nb content.

It has been reported that the formation of sub-grain boundary originates from the deformation of dendrite induced by the thermal stress generated by the precipitated phase of LAGBs[39]. Unlike the traditional casting process, the laser deposition process avoids the macro-segregation of composition, but, the composition segregation between dendrites still exists. The enrichment of elements and the formation of precipitated phases will inevitably lead to the

Table 2 Calculated $m_l(k-1)$ values of elements in titanium alloys[37–38]

Element	m	k	Maximum of c_0/wt%	$m_l(k-1)$
Al	−1.7	~1	20	0
V	−2	~1	12	0
Sn	−1.8	~1	35	0
Zr	−2.3	~1	55	0
Mo	6.5	2	30	6.5
Si	−28	0.333	4	18.7
Nb	13.3	1.5	15	6.6

micro-change of the lattice structure of the matrix and the formation of secondary residual stress, which motivates the formation of sub-structure inside the large columnar grains. Fig. 7 displays SEM images and EDS maps of the laser-deposited premixed titanium alloy powders with the Ti_2AlNb proportion of 50wt%. The width of the river-like sub-grains ranges from 20 μm to 70 μm and the thickness of sub-grain boundaries is about 1.2 μm, as shown in Fig. 7a–7b. The strong white contrast between the boundaries and interior of the sub-grains indicates the enrichment of elements at the sub-grain boundaries and the formation of precipitated phases.

EDS maps (Fig. 7c – 7e) reveal that the Ti, Al and Nb elements dominate the chemical composition of the sub-grain boundary. The element composition of the point A and point B in Fig. 7b is shown in Table 3. When B2 matrix phase is precipitated from the liquid phase during solidification, Nb and Al elements will be enriched at the grain boundary and sub-grain boundary in large quantities. It can be concluded that the observed white and bright precipitate phase is the fine acicular α_2 phase or O phase with the Al element content above 12at%.

Table 3 EDS analysis of marked points in Fig.7b (at%)

Point	Ti	Al	Nb
A	66.25	17.01	16.10
B	71.72	15.17	12.16

When α_2 phase or O phase is precipitated from B2 matrix phase, the system always attempts to reach the lower free energy state due to the differences in chemical composition or crystal structure between the new phase and the parent phase. The interface energy between the precipitate phase and the matrix phase is higher than that of B2 matrix phase. Therefore, α_2 phase or O phase tend to form near existing defects (such as dislocations and faults) or grain boundaries to reduce interface energy, thus promoting the formation of sub-grain structures.

2.4 Formation of sub-grain structure induced by stacking faults

To further analyze the structure of precipitate phase and formation characteristic of sub-grain boundary inside each individual large B2 grains, TEM images of the laser-deposited premixed titanium alloy powders with 50wt% Ti_2AlNb are observed, as shown in Fig. 8. The high density of stacking faults (orange arrows) in B2 matrix and sub-grain boundaries (green dashed lines) can be observed from the brightfield (BF) images in Fig. 8a–8b. The stacking faults with (011) and $(0\bar{1}1)$ slip stacking fault planes are confirmed by high-resolution TEM (HRTEM) images and selected area electron diffraction (SAED) pattern with streaks, as shown in Fig. 8c – 8e. The thermal stress is considered as the main reason for the formation of stacking faults during the rapid solidification process[40]. Although the subsequent multiple deposition layers have the effect of stress release annealing on the previous deposition layers, the heat-affected zone is small due to the

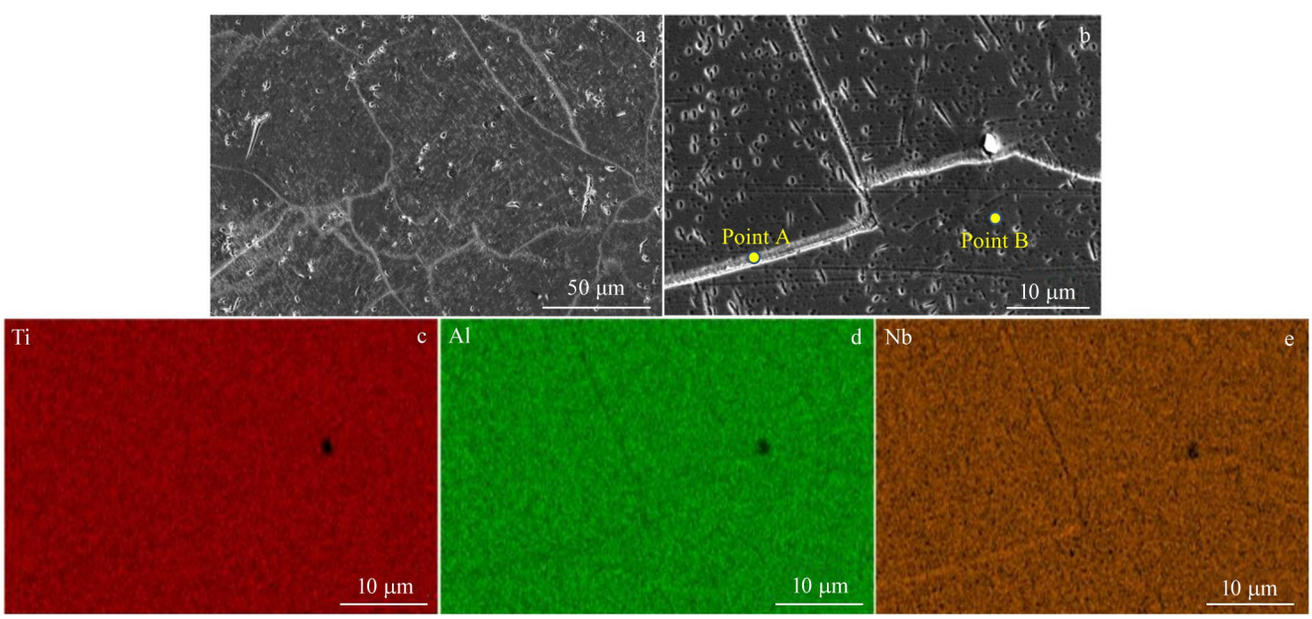

Fig.7 SEM images (a–b) and EDS element mappings (c–e) of laser-deposited premixed titanium alloy powders with Ti_2AlNb proportion of 50wt%

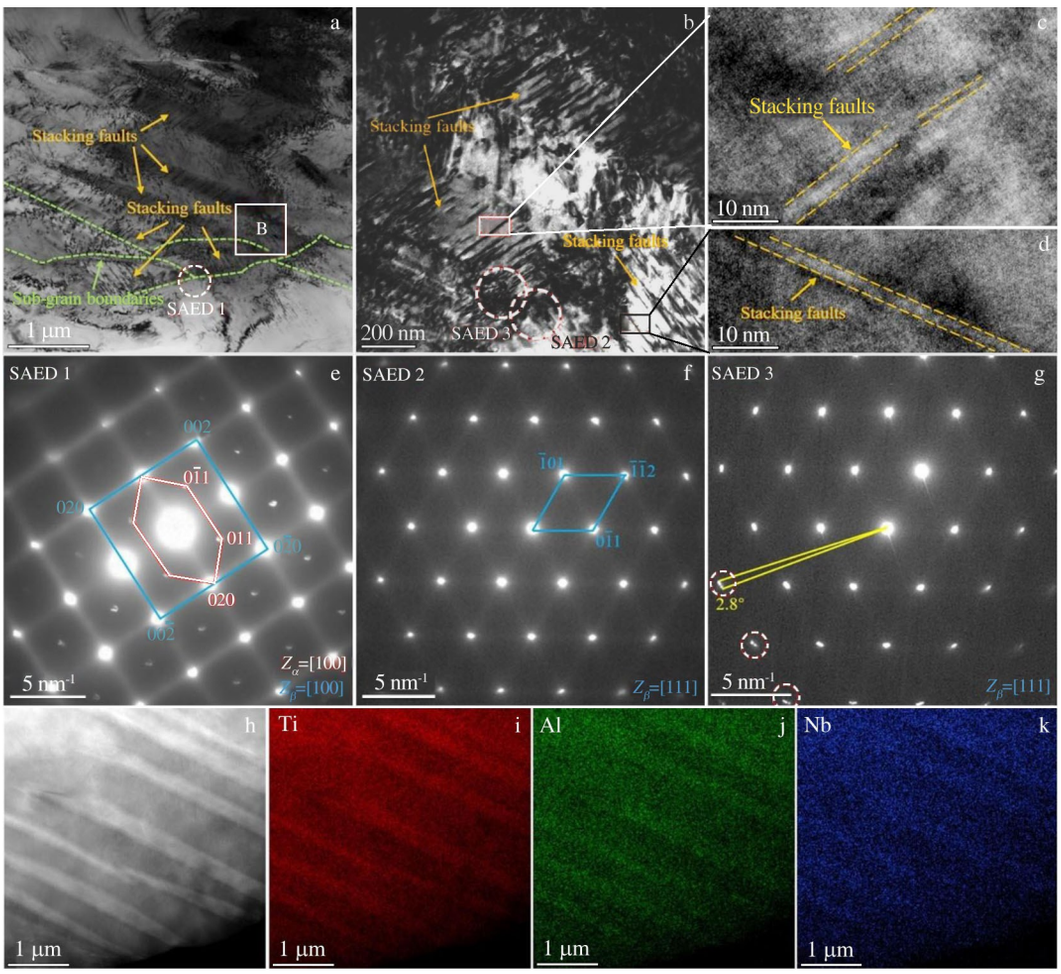

Fig.8 BF-TEM image of stacking faults and sub-grain boundaries laser-deposited premixed titanium alloy powders with Ti_2AlNb proportion of 50wt% (a); magnified morphology of zone B in Fig.8a (b); HRTEM images of marked rectangular regions in Fig.8b (c–d); SAED patterns of circled areas in Fig.8a–8b (e–g); HADDF-STEM image (h) and corresponding EDS element mappings (i–k) of stacking faults and composition micro-segregation

rapid heating rate and high scanning speed, and new thermal stress will be generated with the rapid cooling process. Thus, irregular atomic arrangement and local stacking faults are formed. The stacking faults may serve as the boundary that divide the sub-grains, and form sub-grain structures with subsequent in-situ heat treatment or self-diffusion.

As shown in Fig.8e, the ordered orthorhombic O phase can be observed, which is precipitated from B2 matrix with ordered body centered cubic structure. The formation of O phases may be accompanied by the generation of stacking faults, which can stabilize at the phase interface and lead to the appearance of sub-grain structures.

In Fig.8f–8g, the misorientation angle near the sub-grain boundaries is 2.8°, which is slightly deviated from standard B2 SAED pattern with [111] zone axis (seen red dashed circles), implying that the LAGBs tend to form at the stacking faults region. In addition, the high-angle annular dark-field scanning transmission electron microscope (HAADF-STEM) characterizations suggest that the formation elements of O phase (Ti, Al and Nb) are mainly concentrated in the stacking faults, which confirm again the existence of micro-segregation of composition. Composition segregation may enhance the local stress state, leading to intensified lattice distortion and the generation of stacking faults. To sum up, the precipitation of O phase due to the micro-segregation of composition and the stacking faults provides the driving force for the sub-grain structures.

3 Conclusions

1) The river-like sub-grain structures are formed inside equiaxed B2 grains of the laser-deposited premixed titanium alloy powders with the proportion of Ti_2AlNb above 40wt% . Whereas needle-like structures are formed within columnar β grains with the proportion of Ti_2AlNb below 40wt%.

2) The decrease in laser power and scanning speed can accelerate the formation of sub-grain structures. EBSD results indicate the higher local misorientation (maximum value of 7.07°) and the internal stress are mainly focused on the sub-grain structures.

3) The enrichment of Ti, Al and Nb elements at the sub-grain boundaries leads to micro-segregation of

composition and promotes the precipitation of O phase from B2 matrix.

4) The stacking faults induced by the thermal stress during the rapid solidification are also responsible for the formation of sub-grain structure.

References

1 Otte J A, Zou J, Dargusch M S. *Journal of Materials Science & Technology*[J], 2022, 118: 114

2 Tao X W, Jiang Y X, Xu Z Y *et al. Journal of Alloys and Compounds*[J], 2023, 954: 170212

3 Wang Guodong, Wang Dan, Xue Shaobo *et al*. *Titanium Industry Progress*[J], 2023, 40(1): 16 (in Chinese)

4 Zhang Jikui, Chen Baihui, Zhang Xiang. *Rare Metal Materials and Engineering*[J], 2018, 47(3): 920 (in Chinese)

5 Duan X N, Wang S R, Yang H N *et al. Journal of Materials Research and Technology*[J], 2023, 26: 1677

6 Su Y Y, Wang Z F, Xie J C *et al. Materials Science and Engineering A*[J], 2021, 817: 141355

7 Wang X, Zhang S, Wang Z Y *et al. Materials Today Communications*[J], 2022, 31: 103778

8 Chen H X, Liu Z Y, Cheng X *et al. Journal of Alloys and Compounds*[J], 2021, 875: 159946

9 Attar H, Bönisch M, Calin M *et al. Acta Materialia*[J], 2014, 76: 13

10 Liu Shichao, Lei Pengfei, Liu Min *et al. Rare Metal Materials and Engineering*[J], 2021, 50(10): 3543

11 Bambach M, Sizova I, Sydow B *et al*. *Journal of Materials Research and Technology*[J], 2020, 282: 116689

12 Dolev O, Osovski S, Shirizly A. *Additive Manufacturing*[J], 2021, 37: 101657

13 Bermingham M J, Kent D, Zhan H *et al. Acta Materialia*[J], 2015, 91: 289

14 Qi Zhongliang, Chen Jing, Zhou Qingjun *et al. Applied Laser*[J], 2020, 40: 214 (in Chinese)

15 Ji F L, Hu Z Q, Qin X P *et al. Journal of Materials Science*[J], 2023, 58: 2381

16 Wu Dongjiang, Yuan Shijun, Yu Chao *et al. Rare Metal Materials and Engineering*[J], 2021, 50(1): 78

17 Hicks C, Konkova T, Blackwel P. *Materials Characterization*[J], 2020, 170: 110675

18 Zhang K, Tian X, Bermingham M *et al. Materials & Design*[J], 2019, 184: 108191

19 Bermingham M J, McDonald S D, Dargusch M S *et al. Materials Science and Engineering A*[J], 2018, 719: 1

20 Chong Y, Gholizadeh R, Yamamoto K *et al. Scripta Materialia*[J], 2023, 230: 115397

21 Lu T, Cui Y N, Xue L N *et al. Journal of Materials Science*[J], 2021, 56: 12438

22 Wang S X, Gan X M, Zheng R *et al. Scripta Materialia*[J], 2023, 229: 115379

23 Zhang D Y, Qiu D, Gibson M A *et al. Nature*[J], 2019, 576(2019): 91

24 Han J, Zhang G Y, Chen X Y *et al. Journal of Materials Processing Technology*[J], 2022, 310: 117759

25 Mereddy S, Bermingham M J, Kent D *et al. JOM*[J], 2018, 20: 1670

26 Traxel K D, Bandyopadhyay A. *Additive Manufacturing*[J], 2020, 31: 101004

27 Pang X T, Xiong Z H, Sun J H *et al. Materials Letters*[J], 2022, 326: 132949

28 Wang X, Zhang L J, Ning J *et al. Additive Manufacturing*[J], 2021, 45: 102045

29 Bermingham M J, StJohn D H, Krynen J *et al. Acta Materialia*[J], 2019, 168: 261

30 Chao Q, Mateti S, Annasamy M *et al. Additive Manufacturing*[J], 2021, 46: 102173

31 Zhou Qingjun, Qi Zhongliang, Yan Zhenyu *et al. Applied Laser*[J], 2020, 40(3): 421 (in Chinese)

32 Saeidi K, Gao X, Zhong Y *et al. Materials Science and Engineering A*[J], 2015, 625: 221

33 Cao Y, Bai P C, Liu F *et al. Materials*[J], 2020, 13(2): 340

34 Zhao Y N, Ma Z Q, Yu L M *et al. Journal of Materials Processing Technology*[J], 2021, 68: 184

35 Salman O O, Gammer C, Chaubey A K *et al. Materials Science and Engineering A*[J], 2019, 748: 205

36 Liu Yantao, Gong Xinyong, Liu Mingkun et *al. Chinese Journal of Lasers*[J], 2014, 41(1): 0103005 (in Chinese)

37 Bermingham M J, McDonald S D, Dargusch M S *et al. Journal of Materials Research*[J], 2008, 23(1): 97

38 Eastion M, StJohn D. *Metallurgical and Materials Transactions A*[J], 2005, 36: 1911

39 Siredey N, Boufoussi M, Denis S *et al. Journal of Crystal Growth*[J], 1993, 130(1–2): 132

40 Zhang Y C, Song R B, Wang Y J *et al. Scripta Materialia*[J], 2023, 229: 115372

激光沉积预混合的近α钛合金和Ti_2AlNb合金粉末中成分偏析与层错诱导亚晶结构形成

刘　娜[1,2]，赵张龙[1]，刘郁丽[1,2]，冯凯凯[3]，查小晖[3]，李　璞[3]，徐文馨[1]，杨海鸥[1,2]，赖运金[4]

(1. 西北工业大学 材料学院，陕西 西安 710072)

(2. 西北工业大学 凝固技术国家重点实验室，陕西 西安 710072)

(3. 中国航发湖南动力机械研究所 发动机研发部，湖南 株洲 412002)

(4. 西安欧中材料科技有限公司，陕西 西安 710018)

摘　要：通过激光沉积在近α钛合金基板上制备了不同比例的预混合近α钛合金和Ti_2AlNb合金粉末，并对2种粉末的微观组织演变和结构特征进行了分析和讨论。结果表明，Ti_2AlNb含量在40%（质量分数，下同）以上的激光沉积预混合钛合金粉末的等轴B2晶粒内形成了许多河流状亚晶粒结构，而Ti_2AlNb含量在40%以下的粗柱状β晶粒内则呈现针状结构。值得注意的是，降低激光功率和扫描速度可以促进亚晶粒结构的形成。基于实验结果的分析可以推断出，这种亚晶粒结构的形成不仅与亚晶界成分微偏析导致的O相析出有关，还与激光沉积过程中内应力诱导的堆垛层错密不可分。

关键词：激光沉积；预混合钛合金粉末；亚晶结构；成分偏析；堆垛层错

作者简介：刘　娜，女，1994年生，博士生，西北工业大学材料学院，陕西 西安 710012，电话：029-88460845，E-mail：2020100872@mail.nwpu.edu.cn